CHEMISTRY

Dynamical interference in the vibronic bond breaking reaction of HCO

Shanyu Han[1,2]*, Xianfeng Zheng[3,4]*, Steve Ndengué[5], Yu Song[4], Richard Dawes[5]†, Daiqian Xie[1,6,7]†, Jingsong Zhang[4]†, Hua Guo[2]†

First-principles treatments of quantum molecular reaction dynamics have reached the level of quantitative accuracy even in cases with strong non–Born-Oppenheimer effects. This achievement permits the interpretation of puzzling experimental phenomena related to dynamics governed by multiple coupled potential energy surfaces. We present a combined experimental and theoretical study of the photodissociation of formyl radical (HCO). Oscillations observed in the distribution of product states are found to arise from the interference of matter waves—a manifestation analogous to Young's double-slit experiment.

INTRODUCTION

The wave nature of quantum particles gives rise to interference phenomena, which are analogs of the optical interference in Young's double-slit experiment. When a particle reaches a destination via more than one path, the phase associated with each path is generally different. As the observable intensity is the squared sum of all contributing amplitudes, the phase differences lead to oscillatory patterns in intensity (*1*). While such wave-like behaviors are well known in physics, manifestations of interference in molecular reactions are rare, as they require distinct pathways with nearly equal probabilities. One such example is the inelastic scattering of NO by Ar (*2*, *3*), where a Δj = even propensity can be attributed to the weakly broken symmetry of the diatom (*4*). Various forms of interferences have also been found in reactive scattering (*5*–*7*). More closely related to the current work is the photodissociation of water in its $\tilde{B}$ band, where nonadiabatic transitions between the $\tilde{B}^1A'$ and $\tilde{X}^1A'$ states of H_2O near two conical intersections (HOH and HHO) provide distinct dissociation pathways leading to the same OH + H products, manifested by oscillations in the OH rotational state distribution (*8*). Here, we describe observations of interference in another chemical process, governed by Renner-Teller (RT) electronic state degeneracy at linearity, the photodissociation of HCO. In this case, photoexcitation from the ground electronic state (with a bent equilibrium geometry) to the lowest excited electronic state (with a linear equilibrium geometry) gives rise to a strong bending excitation. The two electronic states are degenerate at linearity, and once a nonadiabatic transition is made

[1]Institute of Theoretical and Computational Chemistry, Key Laboratory of Mesoscopic Chemistry, School of Chemistry and Chemical Engineering, Nanjing University, Nanjing 210093, China. [2]Department of Chemistry and Chemical Biology, University of New Mexico, Albuquerque, NM 87131, USA. [3]Anhui Province Key Laboratory of Optoelectric Materials Science and Technology, Department of Physics, Anhui Normal University, Wuhu, Anhui 241000, China. [4]Department of Chemistry, University of California, Riverside, Riverside, CA 92521, USA. [5]Department of Chemistry, Missouri University of Science and Technology, Rolla, MO 65409, USA. [6]Synergetic Innovation Center of Quantum Information & Quantum Physics (CAS), University of Science and Technology of China, Hefei, Anhui 230026, China. [7]State Key Laboratory of Molecular Reaction Dynamics and Center for Theoretical Computational Chemistry, Dalian Institute of Chemical Physics, Chinese Academy of Sciences, Dalian 116023, China.
*These authors contributed equally to this work.
†Corresponding author. Email: dawesr@mst.edu (R.D.); dqxie@nju.edu.cn (D.X.); jingsong.zhang@ucr.edu (J.Z.); hguo@unm.edu (H.G.)

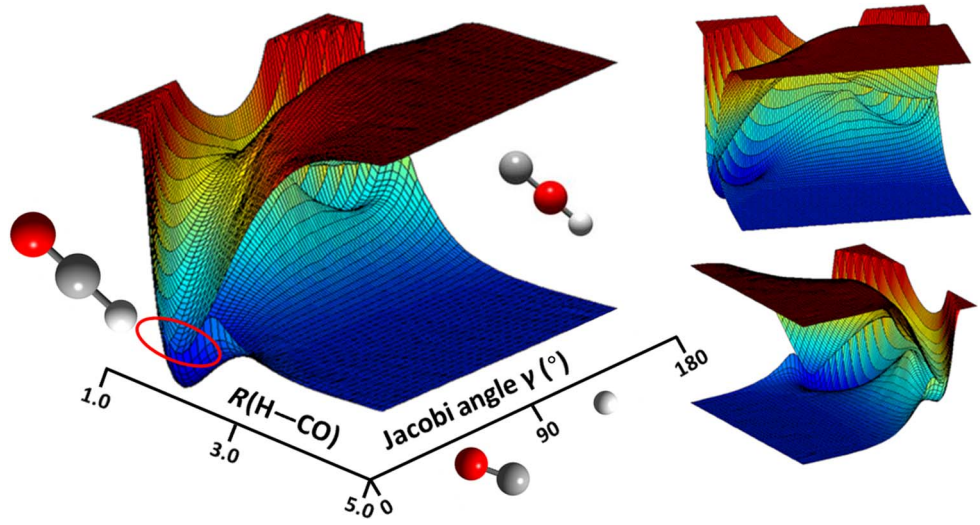

Fig. 1. Surface plots of the coupled $\tilde{X}$ and $\tilde{A}$ states of the formyl radical relevant to photodissociation dynamics. The CO bond distance is held fixed (r_{CO} = 1.18 Å), while the plots illustrate the behavior of the PESs as a function of *R* and γ (Jacobi coordinates, angstroms, and degrees). Seams of degeneracy are noticeable for collinear geometries of HCO (0°) and HOC (180°). The region of the seam for collinear HCO (γ = 0) most relevant to the dynamics is highlighted by a red oval. Top and bottom panels on the right show rotated perspectives of the same plot.

to the ground state, dissociation (to CO + H) occurs with considerable rotational excitation of CO. Moreover, the complex topography of the ground electronic state leads to interference between different paths to the same rotational product states, seen as oscillations in the CO rotational distribution.

The formyl radical (HCO) is an important combustion intermediate, which serves as the primary source of H in the chain initiation of hydrocarbon combustion. It also plays important roles in atmospheric and interstellar chemistry. The $\tilde{A}^2A''\leftarrow\tilde{X}^2A'$ absorption band consists of a long progression of diffuse features, stemming from the bent-to-linear transition (*9*). Interestingly, the linear $\tilde{A}^2A''$ state and bent $\tilde{X}^2A'$ state become degenerate at linearity as an RT $^2\Pi$ pair (*10*), which is subject to a type of non–Born-Oppenheimer coupling between the molecular rotational angular momentum (K) and the electronic angular momentum (Λ) (*11*). The potential energy surfaces (PESs) of these two states (*12*) are shown in Fig. 1, in which the seams of degeneracy for linear geometries are visible. For $K > 0$, this vibronic coupling facilitates rapid predissociation of the $\tilde{A}^2A''$ vibronic levels above the H + CO dissociation asymptote (*13*, *14*). The CO product from HCO ($\tilde{A}^2A''$) photodissociation has been detected by Houston and coworkers and has been found to have rather high (up to $j = 50$) rotational excitation, while its vibrational excitation depends on the initial CO mode excitation in the parent molecule (*15*–*18*). The product energy disposal can be rationalized by the anisotropy of the ground $\tilde{X}^2A'$ state PES, which has an equilibrium valence bond angle of $\theta = \sim 125^\circ$. The PES thus exerts a strong torque on the CO fragment as it emerges from the collinear degeneracy seam, as demonstrated by previous dynamical studies of the dissociation (*19*–*21*).

We report here a new investigation of the dynamics and CO internal state distributions, recorded following photoexcitation of HCO at several wavelengths.

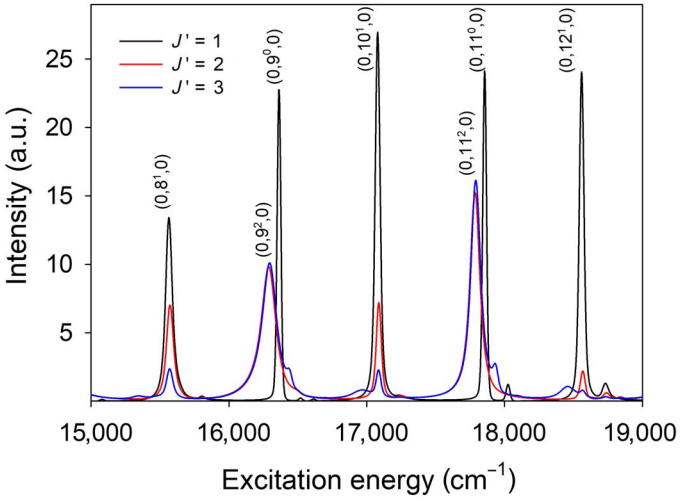

Fig. 2. Calculated absorption spectrum of the 2_{02} state (the J' label refers to the upper state in the transition) of HCO. The extremely close agreement between calculated and recorded positions and widths is given in table S1. a.u., atomic units.

RESULTS

In Fig. 2, the calculated absorption spectrum is shown for the 2_{02} state of HCO ($\tilde{X}^2A'$), which has a substantial population ($P = 0.18$, assuming Boltzmann) at the estimated experimental temperature of 20 K. In agreement with experiments (*9*, *13*), the spectrum is dominated by a pure bending progression, denoted as $(0, n_2'^{K'}, 0)$. Strictly speaking, because of the Coriolis coupling, K' is not a good quantum number, but it can still be used to assign the peaks. It is apparent that the resonance width increases drastically with K' because of increased RT coupling (*10*). As shown in table S1, the calculated transition frequencies and linewidths of the resonances are in excellent agreement with the existing experimental data, further validating the PESs.

In Fig. 3, the measured CO ($v = 0$) product rotational state distributions following excitation to the HCO ($\tilde{A}^2A''$) $(0,10^1,0)$ and $(0,12^1,0)$ states are compared with the calculated ones. The oscillatory structure in the experimental distributions noted previously by Houston and coworkers (*15*–*18*) is unambiguously established and extended to the low-j region owing to the increased and uniform

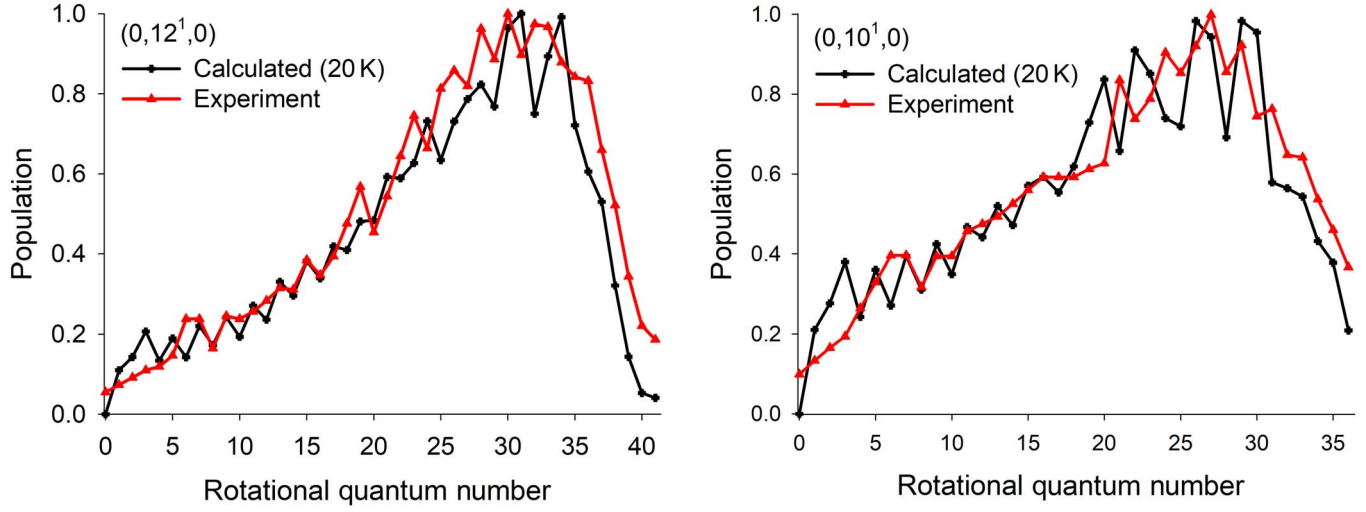

Fig. 3. Comparison of calculated and measured CO rotational distributions. The observed oscillatory and highly excited inverted product distributions are closely reproduced in the calculations. Simulated distributions for pure initial states (or lower beam temperatures) are even more oscillatory (see the Supplementary Materials).

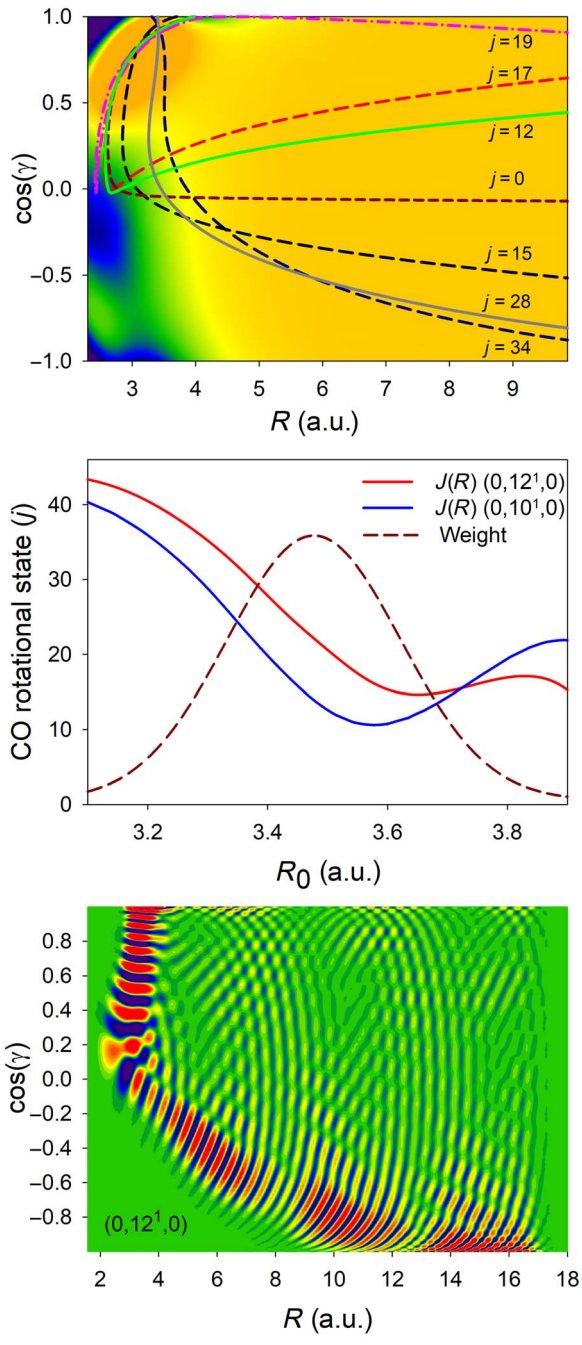

Fig. 4. Insight into the origin of quantum interference in the reaction product distribution is obtained by a comparison of rigorous quantum scattering calculations with quasi-classical trajectories (for details of the calculations, see the main text and the Supplementary Materials). Bottom: Interference fringes are seen in the quantum wave function as it leaves the molecular region, moving toward the asymptotic product channels. **Top and middle:** Illustration of how a rotational rainbow effect is predicted as classical trajectories with different phases contribute to the same CO product states labeled by *j*'s. Energies in the top panel are relative to the minimum on the ground electronic state. The square of the upper-state wave function provides the weight of the coordinate *R* (initially at R_0). The Jacobi coordinates are used in which *r* and *R* denote the C-O distance and distance between H and the CO center of mass, while γ is the enclosing angle.

sensitivity of the high-*n* Rydberg-atom time-of-flight (HRTOF) technique and the CO background free product detection. The simulated product distributions obtained as thermal averages over initial rotational states (assuming 20 K beam temperature) are in very good agreement with the experiment. Any remaining differences between the measured and calculated distributions are most likely due to the strong sensitivity of the interference effect to subtleties of the PESs as well as to the experimental conditions. In fig. S7, the individual (initial rotational state) components are given. There, it can be seen that the rotational state distributions calculated from pure parent states are significantly more oscillatory than the experimental ones recorded at ~20 K, similar to those reported in earlier calculations (*20*). The less pronounced oscillation mainly reflects averaging over the initial rotational states but perhaps also contributions from broadening mechanisms (convolution of computed spectra with assumed linewidth parameters often leads to more similar comparisons).

DISCUSSION

Let us now focus on the oscillations of the CO rotational state distributions. To gain insight into the dynamics and possible interference effects, we analyze trajectories on the ground-state PES originating from linearity where the RT coupling takes place. For this purpose, the $(0,12^1,0)$ state is chosen. In Fig. 4 (top panel), a few two-dimensional representative trajectories are shown on the $\tilde{X}^2A'$ state PES, in which the C-O distance is fixed at its equilibrium geometry ($r_{CO} = r_0 = 1.18$ Å). This is a reasonable approximation as CO vibration is nearly a spectator in the dissociation. To mimic the RT dissociation process, all trajectories were started at linearity with different R_0 values and zero momentum in the *R* direction. The available kinetic energy is exclusively placed in the angular coordinate: $j_0 = \sqrt{2m_r r_0^2(E-V)}$. It is clear from the figure that typical trajectories are first attracted to the HCO well but are subsequently deflected by the isomerization barrier between HCO and HOC and then eventually dissociate. Other details of the trajectory calculations can be found in the Supplementary Materials.

Although such an oversimplified classical model is not expected to generate quantitative results, the trajectories are useful nonetheless to shed light on the dissociation dynamics, particularly the interference effect, as explained below. It is interesting to note that various trajectories arrive at the same final rotational angular momentum, despite the fact that they sampled different parts of the PES and hence arrive out of phase. To better illustrate this effect, the excitation function, namely, the dependence of the final CO rotational quantum number on the initial R_0 position, is plotted in Fig. 4 (middle panel). It is clear from the figure that the excitation function has a turning point near $R_0 \sim 3.6$ atomic units, which is well within the range of the $(0,12^1,0)$ wave function (as also shown in the same figure). The presence of this turning point $\left(\frac{\partial j_{CO}}{\partial R_0} = 0\right)$ suggests a singularity in the classical rotational excitation function. In this so-called rotational rainbow effect, trajectories with different initial positions lead to the same final rotational state (*22*). The quantum mechanical equivalent of the classical rainbow effect manifests in oscillations in the CO rotational state distribution, resulting from the constructive and destructive interference among the corresponding "quantum trajectories" because of the different dynamical phases associated with them (*6*). Although absent in the classical product rotational state distribution, the interference effect can be seen in the corresponding wave function in Fig. 4 (bottom panel), where

waves emanating from different sources interfere as manifested by nodes. The interferences eventually lead to the oscillatory CO rotational state distribution in Fig. 3.

The interference effect reported here differs from that observed in the photodissociation of $H_2O(\tilde{B})$ (*8*) because there, the interference is between trajectories emanating from the HOH and HHO conical intersections. In the present case, on the other hand, the interference effect stems from the same source (RT coupling at linearity). Similar to the recently discussed scenario found in the H + D_2 reactive scattering (*6*), these interference effects can all be traced back to the features on an adiabatic PES, which dictate the nuclear dynamics.

To summarize, we report quantum state-to-state dynamics in a prototypical system in which observed oscillations in the product-state distribution are attributed to an interference effect stemming from unique features on the ground-state PES of the system. As a result, these interference effects are exquisitely sensitive to the PES and thus can be used to probe dynamically important regions of the reactive PES.

MATERIALS AND METHODS

Experimental

The HRTOF technique (*23*–*27*) was used to obtain the H + CO product center-of-mass (CM) translational energy and angular distributions. A pulsed HCO beam was generated by photolyzing a ~2% mixture of acrolein in Ar with the 193-nm radiation of an ArF excimer laser focused in front of the pulse nozzle. The HCO radicals produced were entrained in the molecular beam and subsequently cooled (to ~20 K) by supersonic expansion. The radical beam was collimated and then crossed with the visible photolysis radiation from a Nd:YAG pumped dye laser (defined here as the photolysis laser). This photolysis laser radiation was slightly focused and properly delayed with respect to the 193-nm radical production laser but preceded the H-atom product probe lasers; its polarization can be rotated by a Fresnel-Rhomb achromatic λ/2 plate for product angular distribution studies. Hydrogen atoms produced from photodissociation were first excited to the 2^2P level by a 121.6-nm Lyman-α (L-α) radiation generated by tripling a 364.7-nm dye-laser output in Kr (values given are vacuum wavelengths). The H atoms were further excited to a high-*n* Rydberg level by the 366.2-nm output of another dye laser (Rydberg probe laser). A small fraction of the radiatively metastable Rydberg atoms drifted with their nascent velocities to a microchannel plate detector that was perpendicular to the molecular beam, and were detected as ions after being field ionized in front of the detector. The nominal flight length was 37.1 cm. The accumulated H-atom TOF spectra represented 50,000 to 100,000 laser firings. Because the HRTOF tagging technique gives high resolution and uniform detection sensitivity for the kinetic energy of the H fragment and was rid of the CO background interference, the observed CO rotational-vibrational state distributions were well resolved and extended to the low-*j* states and can be more reliably interpreted than those reported previously (*15*–*18*). It is clear from these experimental data that the CO rotational state distributions exhibit pronounced and reproducible oscillations in nascent product states, extending through the low-*j* excitation range (see Fig. 3). More details of the experiments and results are provided in the Supplementary Materials.

Theoretical

To understand these oscillatory features, we performed full-dimensional wave packet studies. While ab initio ground-state PESs of this system have been reported by several groups (*28*–*30*), fully coupled PESs of the lowest few electronic states are rare (*20*, *31*). The results reported here were obtained on the most recent coupled PESs determined from high-level ab initio calculations (*12*), proven to be considerably more accurate than the previous PESs (*20*). More details of these calculations are provided in the Supplementary Materials. Briefly, the RT coupling was treated using the theoretical approach of Petrongolo (*32*) and Goldfield *et al.* (*19*), as implemented in our recent work (*33*). The strong Coriolis coupling was included explicitly while neglecting spin-orbit coupling. The photoexcitation was simulated using the Condon approximation by exciting the thermally populated low-lying rotationally excited but vibrationally cold eigenfunctions (labeled $J_{K_aK_c}$) from the ground $\tilde{X}^2A'$ electronic state PES, up onto the $\tilde{A}^2A''$ state PES according to rigorous selection rules (the use of integer labels for J in this spin doublet system is due to the neglect of spin-orbit coupling) (*34*). They were then propagated on both coupled electronic states using the Chebyshev propagator (*35*) until reaching the H + CO dissociation asymptote, where the CO rotational-vibrational state distributions were determined by projecting the wave packet onto asymptotic product-state bases on the $\tilde{X}^2A'$ state PES (*36*).

SUPPLEMENTARY MATERIALS

Supplementary material for this article is available at http://advances.sciencemag.org/cgi/content/full/5/1/eaau0582/DC1

Section S1. Experimental
Section S2. Electronic structure and PES
Section S3. Quantum dynamics
Section S4. Classical trajectory calculations
Table S1. Comparison of the calculated and measured (*5*) positions and widths of resonances.
Fig. S1. Resonance enhanced multiphoton ionization spectrum of the HCO $\tilde{B}^2A'(0,0,2) \leftarrow \tilde{X}^2A'(0,0,0)$ transition.
Fig. S2. H-atom photofragment yield spectrum of the HCO radical as a function of photolysis excitation wavelength around the $\tilde{A}^2A''(0,12^1,0) \leftarrow \tilde{X}^2A'(0,0^0,0)$ transition.
Fig. S3. CM translational energy distributions $P(E_T,\theta)$'s and anisotropy parameter β of the H + CO products from photodissociation of the $\tilde{A}^2A''(0,12^1,0)$ vibronic state.
Fig. S4. CM translational energy distributions $P(E_T,\theta)$'s and anisotropy parameter β of the H + CO products from photodissociation of the $\tilde{A}^2A''(0,10^1,0)$ vibronic state.
Fig. S5. Internal energy and rotational state distributions of the CO ($X^1\Sigma^+$, υ = 0) product from photodissociation of the $\tilde{A}^2A''$ vibronic states.
Fig. S6. The convergence of the *X* and *A* states toward their collinear degeneracy is shown at the minimum of the seam [adapted from (*12*)].
Fig. S7. Simulated CO product distributions.
Fig. S8. Plot of typical trajectories shown over the contours of the ground-state PES in the plane with CO distance fixed.
References (*37*–*62*)

REFERENCES AND NOTES

1. C. Cohen-Tannoudji, B. Diu, R. Lalo, *Quantum Mechanics* (Wiley, 1977).
2. C. J. Eyles, M. Brouard, C.-H. Yang, J. Kłos, F. J. Aoiz, A. Gijsbertsen, A. E. Wiskerke, S. Stolte, Interference structures in the differential cross-sections for inelastic scattering of NO by Ar. *Nat. Chem.* **3**, 597–602 (2011).
3. B. Nichols, H. Chadwick, S. D. S. Gordon, C. J. Eyles, B. Hornung, M. Brouard, M. H. Alexander, F. J. Aoiz, A. Gijsbertsen, S. Stolte, Steric effects and quantum interference in the inelastic scattering of NO(X) + Ar. *Chem. Sci.* **6**, 2202–2210 (2015).
4. C. W. McCurdy, W. H. Miller, Interference effects in rotational state distributions: Propensity and inverse propensity. *J. Chem. Phys.* **67**, 463–468 (1977).
5. D. X. Dai, C. C. Wang, S. A. Harich, X. Wang, X. Yang, S. Der Chao, R. T. Skodje, Interference of quantized transition-state pathways in the H + D_2 → D + HD chemical reaction. *Science* **300**, 1730–1734 (2003).
6. P. G. Jambrina, D. Herráez-Aguilar, F. J. Aoiz, M. Sneha, J. Jankunas, R. N. Zare, Quantum interference between H + D_2 quasiclassical reaction mechanisms. *Nat. Chem.* **7**, 661–667 (2015).
7. D. Yuan, S. Yu, W. Chen, J. Sang, C. Luo, T. Wang, X. Xu, P. Casavecchia, X. Wang, Z. Sun, D. H. Zhang, X. Yang, Direct observation of forward-scattering oscillations in the H + HD→H_2 + D reaction. *Nat. Chem.* **10**, 653–658 (2018).

8. R. N. Dixon, D. W. Hwang, X. F. Yang, S. Harich, J. J. Lin, X. Yang, Chemical "double slits": Dynamical interference of photodissociation pathways in water. *Science* **285**, 1249–1253 (1999).
9. J. W. C. Johns, S. H. Priddle, D. A. Ramsay, Electronic absorption spectra of HCO and DCO radicals. *Discuss. Faraday Soc.* **35**, 90–104 (1963).
10. R. N. Dixon, The role of inter-state Renner-Teller coupling in the dissociation of triatomic molecules: A time-dependent approach. *Mol. Phys.* **54**, 333–350 (1985).
11. E. Renner, Zur theorie der wechselwirkung zwischen elektronen- und kernbewegung bei dreiatomigen, stabförmigen molekülen. *Z. Phys.* **92**, 172–193 (1934).
12. S. A. Ndengué, R. Dawes, H. Guo, A new set of potential energy surfaces for HCO: Influence of Renner-Teller coupling on the bound and resonance vibrational states. *J. Chem. Phys.* **144**, 244301 (2016).
13. J.-C. Loison, S. H. Kable, P. L. Houston, I. Burak, Photofragment excitation spectroscopy of the formyl (HCO/DCO) radical: Linewidths and predissociation rates of the $\tilde{A}(A'')$ state. *J. Chem. Phys.* **94**, 1796–1802 (1991).
14. S. H. Kable, J.-C. Loison, D. W. Neyer, P. L. Houston, I. Burak, R. N. Dixon, Observation of a parallel recoil distribution from a perpendicular absorption transition in formyl radicals HCO and DCO. *J. Phys. Chem.* **95**, 8013–8018 (1991).
15. S. H. Kable, J.-C. Loison, P. L. Houston, I. Burak, The photochemistry of the formyl radical: Energy content of the photoproducts. *J. Chem. Phys.* **92**, 6332–6333 (1990).
16. D. W. Neyer, S. H. Kable, J.-C. Loison, P. L. Houston, I. Burak, E. M. Goldfield, CO product distributions from the visible photodissociation of HCO. *J. Chem. Phys.* **97**, 9036–9045 (1992).
17. D. W. Neyer, X. Luo, P. L. Houston, I. Burak, CO product distribution from metastable levels of HCO $\tilde{X}^2A'$ prepared by stimulated emission pumping. *J. Chem. Phys.* **98**, 5095–5098 (1993).
18. D. W. Neyer, X. Luo, I. Burak, P. L. Houston, Photodissociation dynamics of state-selected resonances of HCO $\tilde{X}^2A'$ prepared by stimulated emission pumping. *J. Chem. Phys.* **102**, 1645–1657 (1995).
19. E. M. Goldfield, S. K. Gray, L. B. Harding, Quantum dynamics of Renner-Teller vibronic coupling: The predissociation of HCO. *J. Chem. Phys.* **99**, 5812–5827 (1993).
20. A. Loettgers, A. Untch, H.-M. Keller, R. Schinke, H.-J. Werner, C. Bauer, P. Rosmus, Ab initio study of the photodissociation of HCO in the first absorption band: Three-dimensional wave packet calculations including the $\tilde{X}^2A' - \tilde{A}^2A''$ Renner-Teller coupling. *J. Chem. Phys.* **106**, 3186–3204 (1997).
21. J. Weiß, R. Schinke, V. Mandelshtam, Renner–Teller induced photodissociation of HCO in the first absorption band: Determination of linewidths for the $\tilde{A}^2A''$ $K = 0$, 1 states by filter-diagonalization. *J. Chem. Phys.* **113**, 4588–4597 (2000).
22. R. Schinke, J. M. Bowman, in *Molecular Collision Dynamics*, J. M. Bowman, Ed. (Springer, 1983).
23. L. Schnieder, W. Meier, K. H. Welge, M. N. R. Ashfold, C. M. Western, Photodissociation dynamics of H_2S at 121.6 nm and a determination of the potential energy function of SH($A\ ^2\Sigma^+$). *J. Chem. Phys.* **92**, 7027–7037 (1990).
24. G. Amaral, K. Xu, J. Zhang, UV photodissociation dynamics of ethyl radical via the $\tilde{A}\,^2A'(3s)$ state. *J. Chem. Phys.* **114**, 5164–5169 (2001).
25. W. Zhou, Y. Yuan, J. Zhang, State-to-state photodissociation dynamics of OH radical via the $A\,^2\Sigma^+$ state: Fine-structure distributions of the $O(^3P_J)$ product. *J. Chem. Phys.* **119**, 9989–9992 (2003).
26. Y. Song, X. Zheng, W. Zhou, M. Lucas, J. Zhang, Ultraviolet photodissociation dynamics of the *n*-propyl and *i*-propyl radicals. *J. Chem. Phys.* **142**, 224306 (2015).
27. K. Xu, J. Zhang, Photodissociation of the vinyl radical (C_2H_3) via the first excited state: The $C_2H_2(\tilde{X}^1\Sigma_g^+)$+H channel. *J. Chem. Phys.* **111**, 3783–3786 (1999).
28. J. M. Bowman, J. S. Bittman, L. B. Harding, Ab initio calculations of electronic and vibrational energies of HCO and HOC. *J. Chem. Phys.* **85**, 911–921 (1986).
29. H.-J. Werner, C. Bauer, P. Rosmus, H.-M. Keller, M. Stumpf, R. Schinke, The unimolecular dissociation of HCO: I. Oscillations of pure CO stretching resonance widths. *J. Chem. Phys.* **102**, 3593–3611 (1995).
30. A. Zanchet, B. Bussery-Honvault, P. Honvault, Study of the $C(^3P) + OH(X^2\Pi) \rightarrow CO(X^1\Sigma_g^+) + H(^2S)$ reaction: A fully global ab initio potential energy surface of the X^2A' state. *J. Phys. Chem. A* **110**, 12017–12025 (2006).
31. A. Zanchet, B. Bussery-Honvault, M. Jorfi, P. Honvault, Study of the $C(^3P) + OH(X^2\Pi) \rightarrow CO(a^3\Pi) + H(^2S)$ reaction: Fully global ab initio potential energy surfaces of the $1^2A''$ and $1^4A''$ states and nonadiabatic couplings. *Phys. Chem. Chem. Phys.* **11**, 6182–6191 (2009).
32. C. Petrongolo, Nonadiabatic theory of triatomics: General formalism and application to Renner-Teller and conical-intersection effects. *J. Chem. Phys.* **89**, 1297–1308 (1988).
33. S. Y. Lin, H. Guo, B. Jiang, S. Zhou, D. Xie, Non-Born–Oppenheimer state-to-state dynamics of the $N(^2D) + H_2 \rightarrow NH(\tilde{X}^3\Sigma^-) + H$ reaction: Influence of the Renner–Teller coupling. *J. Phys. Chem. A* **114**, 9655–9661 (2010).
34. G. G. Balint-Kurti, M. Shapiro, Photofragmentation of triatomic molecules. Theory of angular and state distribution of product fragments. *Chem. Phys.* **61**, 137–155 (1981).
35. H. Guo, A time-independent theory of photodissociation based on polynomial propagation. *J. Chem. Phys.* **108**, 2466–2472 (1998).
36. B. Jiang, D. Xie, H. Guo, State-to-state photodissociation dynamics of triatomic molecules: H_2O in the *B* band. *J. Chem. Phys.* **136**, 034302 (2012).
37. A. D. Sappey, D. R. Crosley, Laser-induced fluorescence in the $\tilde{B}$–$\tilde{X}$ system of the HCO radical. *J. Chem. Phys.* **93**, 7601–7608 (1990).
38. T. A. Cool, X.-M. Song, Resonance ionization spectroscopy of HCO and DCO. II. The $\tilde{B}\,^2A'$ state. *J. Chem. Phys.* **96**, 8675–8683 (1992).
39. R. Dawes, S. A. Ndengué, Single- and multireference electronic structure calculations for constructing potential energy surfaces. *Int. Rev. Phys. Chem.* **35**, 441–478 (2016).
40. J. M. Brown, D. A. Ramsay, Axis switching in the $\tilde{A}^2A'' - \tilde{X}^2A'$ transition of HCO: Determination of molecular geometry. *Can. J. Phys.* **53**, 2232–2241 (1975).
41. B. Ruscic, updated Active Thermochemical Tables (ATcT) values based on ver. 1.110 of the Thermochemical Network (2012); available at https://ATcT.anl.gov.
42. J. D. Tobiason, J. R. Dunlop, E. A. Rohlfing, The unimolecular dissociation of HCO: A spectroscopic study of resonance energies and widths. *J. Chem. Phys.* **103**, 1448–1469 (1995).
43. S. A. Ndengué, R. Dawes, F. Gatti, H.-D. Meyer, Resonances of HCO computed using an approach based on the multiconfiguration time-dependent Hartree method. *J. Phys. Chem. A* **119**, 12043–12051 (2015).
44. L. Song, A. van der Avoird, G. C. Groenenboom, Three-dimensional ab initio potential energy surface for H–CO($\tilde{X}^2A'$). *J. Phys. Chem. A* **117**, 7571–7579 (2013).
45. T. Shiozaki, G. Knizia, H.-J. Werner, Explicitly correlated multireference configuration interaction: MRCI-F12. *J. Chem. Phys.* **134**, 034113 (2011).
46. H.-J. Werner, P. J. Knowles, G. Knizia, F. R. Manby, M. Schütz, Molpro: A general-purpose quantum chemistry program package. *WIREs Comput. Mol. Sci.* **2**, 242–253 (2012).
47. M. P. Deskevich, D. J. Nesbitt, H.-J. Werner, Dynamically weighted multiconfiguration self-consistent field: Multistate calculations for $F + H_2O \rightarrow HF + OH$ reaction paths. *J. Chem. Phys.* **120**, 7281–7289 (2004).
48. R. Dawes, A. W. Jasper, C. Tao, C. Richmond, C. Mukarakate, S. H. Kable, S. A. Reid, Theoretical and experimental spectroscopy of the S_2 state of CHF and CDF: Dynamically weighted multireference configuration interaction calculations for high-lying electronic states. *J. Phys. Chem. Lett.* **1**, 641–646 (2010).
49. A. Li, D. Xie, R. Dawes, A. W. Jasper, J. Ma, H. Guo, Global potential energy surface, vibrational spectrum, and reaction dynamics of the first excited ($\tilde{A}^2A'$) state of HO_2. *J. Chem. Phys.* **133**, 144306 (2010).
50. R. Dawes, P. Lolur, J. Ma, H. Guo, Communication: Highly accurate ozone formation potential and implications for kinetics. *J. Chem. Phys.* **135**, 081102 (2011).
51. B. J. Barker, I. O. Antonov, J. M. Merritt, V. E. Bondybey, M. C. Heaven, R. Dawes, Experimental and theoretical studies of the electronic transitions of BeC. *J. Chem. Phys.* **137**, 214313 (2012).
52. A. W. Jasper, R. Dawes, Non-Born–Oppenheimer molecular dynamics of the spin-forbidden reaction $O(^3P) + CO(X^1\Sigma^+) \rightarrow CO_2(\tilde{X}^1\Sigma_g^+)$. *J. Chem. Phys.* **139**, 154313 (2013).
53. R. Dawes, D. L. Thompson, Y. Guo, A. F. Wagner, M. Minkoff, Interpolating moving least-squares methods for fitting potential energy surfaces: Computing high-density potential energy surface data from low-density ab initio data points. *J. Chem. Phys.* **126**, 184108 (2007).
54. R. Dawes, X.-G. Wang, A. W. Jasper, T. Carrington Jr., Nitrous oxide dimer: A new potential energy surface and rovibrational spectrum of the nonpolar isomer. *J. Chem. Phys.* **133**, 134304 (2010).
55. M. Majumder, A. S. Ndengué, R. Dawes, Automated construction of potential energy surfaces. *Mol. Phys.* **114**, 1–18 (2016).
56. L. Zhou, B. Jiang, D. Xie, H. Guo, State-to-state photodissociation dynamics of H_2O in the B-band: Competition between two coexisting nonadiabatic pathways. *J. Phys. Chem. A* **117**, 6940–6947 (2013).
57. G. G. Balint-Kurti, Wavepacket theory of photodissociation and reactive scattering. *Adv. Chem. Phys.* **128**, 249–301 (2004).
58. H. Guo, Recursive solutions to large eigenproblems in molecular spectroscopy and reaction dynamics. *Rev. Comput. Chem.* **25**, 285–347 (2007).
59. R. Kosloff, in *Numerical Grid Methods and Their Applications to Schrodinger's Equation*, C. Cerjan, Ed. (Kluwer, 1993), pp. 175–194.
60. J. C. Light, T. Carrington Jr., Discrete-variable representations and their utilization. *Adv. Chem. Phys.* **114**, 263–310 (2000).
61. R. Schinke, Rotational state distributions of H_2 and CO following the photofragmentation of formaldehyde. *J. Chem. Phys.* **84**, 1487–1491 (1986).
62. R. D. Levine, *Molecular Reaction Dynamics* (Cambridge Univ. Press, 2005).

Acknowledgments

Funding: X.Z. acknowledges support from the National Natural Science Foundation of China (grant no. 11674003). D.X. was supported by the National Natural Science Foundation of China (grant nos. 21688102, 21733006, and 21590802) and the National Key Research and Development Program of China (grant no. 2017YFA0206500). J.Z. acknowledges support from the NSF (grant no. CHE-1566636). This research was also supported by the U.S. Department

of Energy Office of Science, Office of Basic Energy Sciences (grant nos. DE-SC0010616 to R.D. and DE-SC0015997 to H.G.). **Author contributions:** All authors designed and conducted the research and participated in writing the manuscript. **Competing interests:** The authors declare that they have no competing interests. **Data and materials availability:** All data needed to evaluate the conclusions in the paper are present in the paper and/or the Supplementary Materials. Additional data related to this paper may be requested from the authors.

Submitted 2 May 2018
Accepted 26 November 2018
Published 4 January 2019
10.1126/sciadv.aau0582

Citation: S. Han, X. Zheng, S. Ndengué, Y. Song, R. Dawes, D. Xie, J. Zhang, H. Guo, Dynamical interference in the vibronic bond breaking reaction of HCO. *Sci. Adv.* **5**, eaau0582 (2019).